Title

Mice Deficient in TAZ (Wwtr1) Demonstrate Clinical Features of Late-Onset Fuchs' Endothelial Corneal Dystrophy

Permalink

https://escholarship.org/uc/item/2hr2q66c

Journal

Investigative Ophthalmology & Visual Science, 64(4)

ISSN

0146-0404

Authors

Leonard, Brian C

Park, Sangwan

Kim, Soohyun

et al.

Publication Date

2023-04-19

DOI

10.1167/iovs.64.4.22

Peer reviewed

Mice Deficient in TAZ (Wwtr1) Demonstrate Clinical Features of Late-Onset Fuchs' Endothelial Corneal Dystrophy

Brian C. Leonard,[1] Sangwan Park,[1] Soohyun Kim,[1] Laura J. Young,[1] Iman Jalilian,[1] Krista Cosert,[1] Xunzhi Zhang,[2] Jessica M. Skeie,[3,5] Hanna Shevalye,[3,5] Nayeli Echeverria,[1] Vanessa Rozo,[1] Xin Gong,[2] Chao Xing,[2] Christopher J. Murphy,[1,4] Mark A. Greiner,[3,5] V. Vinod Mootha,[2,6] Vijay Krishna Raghunathan,[7] and Sara M. Thomasy[1,4]

[1]Department of Surgical and Radiological Sciences, School of Veterinary Medicine, University of California, Davis, Davis, California, United States
[2]McDermott Center for Human Growth and Development/Center for Human Genetics, University of Texas Southwestern Medical Center, Dallas, Texas, United States
[3]Department of Ophthalmology and Visual Sciences, Carver College of Medicine, University of Iowa Hospitals & Clinics, Iowa City, Iowa, United States
[4]Department of Ophthalmology & Vision Science, School of Medicine, University of California, Davis, Davis, California, United States
[5]Iowa Lions Eye Bank, Coralville, Iowa, United States
[6]Department of Ophthalmology, University of Texas Southwestern Medical Center, Dallas, Texas, United States
[7]Department of Basic Sciences, College of Optometry, University of Houston, Houston, Texas, United States

Purpose. We sought to define the role of *Wwtr1* in murine ocular structure and function and determine the role of mechanotransduction in Fuchs' endothelial corneal dystrophy (FECD), with emphasis on interactions between corneal endothelial cells (CEnCs) and Descemet's membrane (DM).

Methods. A *Wwtr1* deficient mouse colony was established, and advanced ocular imaging, atomic force microscope (AFM), and histology/immunofluorescence were performed. Corneal endothelial wound healing was assessed using cryoinjury and phototherapeutic keratectomy in *Wwtr1* deficient mice. Expression of *WWTR1*/TAZ was determined in the corneal endothelium from normal and FECD-affected patients; *WWTR1* was screened for coding sequence variants in this FECD cohort.

Results. Mice deficient in *Wwtr1* had reduced CEnC density, abnormal CEnC morphology, softer DM, and thinner corneas versus wildtype controls by 2 months of age. Additionally, CEnCs had altered expression and localization of Na/K-ATPase and ZO-1. Further, *Wwtr1* deficient mice had impaired CEnC wound healing. The *WWTR1* transcript was highly expressed in healthy human CEnCs comparable to other genes implicated in FECD pathogenesis. Although *WWTR1* mRNA expression was comparable between healthy and FECD-affected patients, WWTR1/TAZ protein concentrations were higher and localized to the nucleus surrounding guttae. No genetic associations were found in *WWTR1* and FECD in a patient cohort compared to controls.

Conclusions. There are common phenotypic abnormalities seen between *Wwtr1* deficient and FECD-affected patients, suggesting that *Wwtr1* deficient mice could function as a murine model of late-onset FECD. Despite the lack of a genetic association between FECD and *WWTR1*, aberrant *WWTR1*/TAZ protein subcellular localization and degradation may play critical roles in the pathogenesis of FECD.

Keywords: corneal endothelial cells (CEnCs), Fuchs' endothelial corneal dystrophy (FECD), TAZ, *WWTR1*/*Wwtr1*, mechanotransduction

Mechanotransduction, the ability by which cells sense and respond to biomechanical properties of their local microenvironment, via altered regulation of signaling pathways and gene expression, plays a critical role in cell fate decisions. Importantly, aberrant alterations of these pathways can lead to the disruptive remodeling of the cytoskeleton, affecting cellular tension, as well as the synthesis of extracellular matrix (ECM) proteins that lead to non-homeostatic changes in the overall composition and stiffness of the ECM.[1] Multiple proteins within the Hippo pathway are

key to mechanotransduction and tissue homeostasis via the regulation of two key proteins: transcriptional co-activator with PDZ-binding motif (gene = *WWTR1* and protein = TAZ) and yes-associated protein (gene = *YAP1* and protein = YAP).[2] Both YAP and TAZ reside in the cytoplasm of the cell under homeostatic conditions; however, upon stimulation (e.g. stiff ECM), YAP and TAZ localize to the nucleus, initiating stress fiber formation and altering the expression of ECM regulatory proteins.[2] Although these two mechanotransducers are often thought to be functionally redundant, multiple studies have demonstrated that TAZ and YAP can behave independently.[3–8]

A previous study from our group investigated the role of *Yap1* in eye structure and function in the mouse. Homozygous knockout mice ($Yap1^{-/-}$) demonstrated embryonic lethality, whereas heterozygous mice ($Yap1^{+/-}$) had a severe ocular phenotype, characterized by microphthalmia, corneal fibrosis, anterior segment dysgenesis, and cataract.[9] Conversely, multiple investigations into TAZ knockout mice ($Wwtr1^{-/-}$) demonstrated partial embryonic lethality with more limited pathologic findings that included renal cysts and lung emphysema.[10–12] Although there are no investigations into the role of *Wwtr1* in ocular development, a previous study demonstrated that chronic inflammatory disease on the ocular surface led to pathologic changes in epithelial differentiation through YAP-TAZ mediated mechanotransduction.[13]

Alterations in the biomechanical properties of both cells and their ECM are commonly found in the context of disease. For example, chronic inflammatory diseases often lead to stiffening of the ECM and resultant tissue fibrosis due to the unregulated matrix deposition, that can compromise cellular and tissue function.[14] However, there are few examples of diseases that result from or lead to softening of the ECM, and Fuchs' endothelial corneal dystrophy (FECD) may be one given the current evidence that exists.[15] FECD is a primary, degenerative disorder characterized by the progressive loss of corneal endothelial cells (CEnCs) over time. The primary role of CEnCs is to keep the cornea in a relatively deturgescent state to maintain corneal transparency, and this is accomplished through Na/K-ATPase pumps to remove water and zonula occludens (ZO-1) to maintain tight junctions, enacting a barrier to prevent entry of aqueous humor fluid from the inside of the eye into the cornea. CEnCs have limited proliferative capacity in vivo such that progressive loss of CEnCs leads to endothelial dysfunction and corneal edema.[16] With chronicity, vision is severely impaired and painful epithelial bullae could develop.[17] One of the hallmark features of FECD are the formation of excrescences of ECM, termed guttae, on Descemet's membrane (DM). The DM is a specialized basement membrane secreted by CEnCs and our knowledge regarding the ultrastructural and biomechanical properties of DM has greatly expanded in recent years.[18] FECD alters the composition of DM with increased deposition of type I and VIII collagen, fibronectin, and laminin leading to the thickening of DM.[19] In FECD-affected corneas, the DM is thicker than that of healthy corneas even in the regions without guttae formation.[15] Furthermore, one study reported that the DM is markedly softer in humans affected with FECD or guttae formation versus unaffected control corneas, although this was reported in dehydrated tissues and has yet to be confirmed independently.[15] The topography of DM could also affect CEnC behavior. Guttae induced a stress response, senescence, endothelial-mesenchymal transition, and cellular apoptosis in an ex vivo study and CEnCs were not able to attach and migrate over the guttae-affected DM, particularly in large-sized guttae.[20,21]

A knowledge gap still exists in our understanding of the bidirectional interaction between CEnCs and DM, specifically in FECD.[22] Whereas the genetic basis underlying most of early-onset and late-onset FECD cases has been determined, there is a need for the identification of appropriate animal models to understand the pathogenesis of FECD and test the efficacy of therapeutic interventions. The current study sought to confirm if biomechanics of DM are indeed altered and further determine the role of *Wwtr1* (a key mechanotransducer) in murine ocular structure and function, with emphasis on the interactions between CEnCs and DM.

MATERIALS AND METHODS

Animals and Genotyping

One male and 1 female wild-type (WT) 129S mice and 1 male and 1 female *Wwtr1* heterozygous ($Wwtr1^{+/-}$) 129S mice were purchased from The Jackson Laboratory and used to generate a colony consisting of WT, $Wwtr1^{+/-}$, and $Wwtr1^{-/-}$ littermates. Genotypes of offspring were confirmed by PCR from genomic DNA isolated from tail tips or ear tissue. DNA was extracted using a commercial DNA extraction kit (DNeasy Blood & Tissue Kit, QIAGEN Sciences, Germantown, MD, USA) following the manufacturer's protocol. Genotyping was performed by PCR analysis, using the primers and cycling parameters recommended by The Jackson Laboratory (Wildtype Forward, 5′-AAA GTT GTG ATG CCC TGG AC-3′; Common Reverse, 5′-TGT TCT TTT CCG GTT TGC TT-3′; Mutant Forward, 5′-GGG AGG ATT GGG AAG ACA AT-3′). PCR products were subjected to agarose gel electrophoresis. WT and $Wwtr1^{-/-}$ mice showed a single amplified DNA fragment (417 bp for WT and 241 bp for $Wwtr1^{-/-}$), whereas both DNA fragments were amplified in $Wwtr1^{+/-}$ mice.

Ophthalmic Examinations and Advanced Ocular Imaging

Ophthalmic examination and advanced ocular imaging were performed using WT, $Wwtr1^{+/-}$, and $Wwtr1^{-/-}$ within 4 different age groups: 2, 6, and 12 months old. For the ophthalmic examinations, the mice were gently manually restrained. A phenol red thread test (PRTT; Zone-Quick, Showa Yakuhin Kako Co., Ltd., Campinas/SP, Brazil) to quantify aqueous tear production, Cochet-Bonnet esthesiometry (Esthesiometer 12/100 mm; Luneau Ophthalmologi) to evaluate corneal sensation and rebound tonometry (Tono-Lab; Icare) to measure intraocular pressure (IOP) were performed. Subsequently, all mice received full ophthalmic examinations using a handheld slit-lamp (Kowa SL15; Kowa Optimed) and indirect ophthalmoscopy (Keeler VANTAGE Plus; Keeler Inc.) with a 90 D indirect lens (Volk Optical, Inc., Mentor, OH, USA). Following examinations, the mice were sedated with an intraperitoneal injection of ketamine (75 mg/kg) and dexmedetomidine (0.25 mg/kg) for advanced ocular imaging. Slit lamp biomicroscopy with digital capture (Hagg-Streit BQ 900 Slit Lamp; Hagg-Streit) was performed to photograph the eyes. Fourier-domain optical coherence tomography (FD-OCT; RTVue 100, software version 6.1; Optovue, Inc., Fremont, CA, USA) with a CAM-S lens (3-mm scan length) and in vivo confocal microscopy (IVCM;

Heidelberg Retinal Tomography 3 in conjunction with the Rostock Cornea Module; Heidelberg Engineering, Heidelberg, Germany) were utilized to measure central corneal thickness (CCT) and endothelial cell density (ECD), respectively, with three representative regions counted for each eye. Animals were euthanized at the aforementioned time points and OD was used for atomic force microscope (AFM) and OS was used for immunofluorescence staining.

Atomic Force Microscopy: *Wwtr1* Mice

Corneal samples were prepared for measurement with AFM as previously described.[23] Briefly, a standard petri dish was coated with a layer of silicone (Sylgard 527, 24 hours cure at room temperature; Dow Corning) and a 2 mm biopsy punch was used to create a window in a 13 mm Thermanox coverslip (Thermo Fisher Scientific). Corneas were incubated in 2.5 mM EDTA in HEPES buffer for 30 minutes and sonicated for 5 minutes to remove endothelial cells. The epithelium was gently removed with a sterile cotton swab to allow for better contact between the tissue sample and the silicone substrate. Radial cuts were made in the cornea to allow the tissue to lie flat and oriented with the exposed DM oriented upward. The periphery of the coverslip was dotted with cyanoacrylate glue and applied over the cornea such that the 2 mm window would grant access to a central portion of the DM and no glue would contact the tissue. The sample was then fully submerged in Dulbecco's Phosphate Buffered Saline (DPBS) to cure the glue and maintain tissue hydration during measurements. All force measurements were done using an Asylum Research MFP-3D-BIO AFM and PNP-TR-50 silicon nitride cantilevers with nominal spring constants of 0.32 N/m and 35 degrees half-angle openings modified with a 5 μm diameter borosilicate bead (Thermo Fisher Scientific). Immediately prior to use, cantilevers were calibrated for the deflection inverse optical lever sensitivity (Defl InVOLS) by indentation in DPBS on glass and then calibrated for the spring constant by the thermal method in DPBS using the Asylum Research software. The maximum indentation force was set at 5 nN. Each cornea was probed at 5 unique locations with 5 force curves collected per location at a scan velocity of 1.98 μm/s. The point of probe contact with the cornea was determined by a masked analyst and the elastic modulus determined by fitting the force curves to the Hertz model for spherical geometry as described previously.[24]

Wwtr1/TAZ Immunofluorescence

Enucleated globes were immersed in 4% paraformaldehyde (PFA) and then corneas were dissected and fixed in 4% PFA for 1 hour at room temperature. After washing with PBS, the tissues were incubated in 0.1% Triton X-100, PBS, and blocking buffer sequentially for 1 hour each at room temperature. Corneas were cut into four to five pie-shaped pieces for the following antibody staining. For ZO-1 and Na,K-ATPase staining, corneal pieces were incubated with primary antibodies against ZO-1 (1:100, Invitrogen, #61-7300) and Na,K-ATPase (1:200, Invitrogen, MA5-32184) in a mixture of blocking buffer overnight at 4°C. Subsequently, tissues were immersed in PBS for 1 hour and incubated with secondary antibodies (Alexa Fluor 488/594 anti-rabbit IgG H&L, 1:200 in a mixture of blocking buffer) for 1 hour at room temperature. Nuclei were finally counterstained with DAPI and whole-mount corneal tissues were mounted endothelial side up on a slide and were imaged using an Axiovert 200M fluorescent microscope (Carl Zeiss Ag, Oberkochen, Germany) with a 20X and a 40X objective.

Transcorneal Cryoinjury

Eight WT, 8 *Wwtr1*^{+/−}, and 5 *Wwtr1*^{−/−} mice at 7 to 8 months of age were used. A 2-mm diameter steel probe immersed in liquid nitrogen for 3 minutes to an approximate temperature of –196°C was applied to the cornea of both eyes for 10 seconds and the cornea was allowed to thaw spontaneously. Following cryoinjury, mice were treated with topical 0.3% ofloxacin twice daily to prevent secondary corneal infection, and buprenorphine (0.05–0.1 mg/kg) was subcutaneously injected twice daily for analgesia until euthanasia. All mice were euthanized on post-injury day 2, and the eyes were enucleated for alizarin red and 5-ethynyl-2′-deoxyuridine (EdU) staining in corneal endothelial wholemount. For successful EdU incorporation, intraperitoneal injection of 50 mg/kg EdU (Sigma-Aldrich, # 900584) was performed in mice 3 to 4 hours prior to euthanasia. After euthanasia, both corneas were dissected, and the right corneas were used for alizarin red staining and the left corneas were used for EdU staining.

For alizarin red staining, corneas were immersed in 0.2% Alizarin red (Electron Microscopy Sciences, 10360) solution and then fixed in 4% PFA. Corneas were placed endothelial side-up on a glass slide and 4 radial cuts were made to allow a flat mount under a coverslip. Alizarin red stained corneal endothelium was imaged using a light microscope and the denuded area where endothelial monolayer has not reformed was measured in mm^2 by ImageJ software (US National Institutes of Health, Bethesda, MD, USA).

For EdU staining, corneas were fixed in 4% PFA for 30 minutes at room temperature. After washing with PBS, the tissues were incubated in 0.1% Triton X-100, PBS, and blocking buffer sequentially for 30 minutes for each. Then, the tissues were incubated with a Click-iT reaction cocktail containing Click-iT reaction buffer, CuSO4, Alexa Fluor 488 Azide, and reaction buffer additive for 30 minutes while protected from light at room temperature (Click-iT EdU Cell Proliferation Kit for imaging, #C10337, Invitrogen). The tissues were washed with PBS and nuclei were counterstained with DAPI. The corneal tissues were mounted endothelial side up on a glass slide and were imaged using an Axiovert 200M fluorescent microscope (Carl Zeiss Ag, Oberkochen, Germany) with a 20X objective. A montage of 20X images was created for each cornea. The total number of EdU-positive endothelial nuclei was counted for each corneal endothelial wholemount.

Phototherapeutic Keratectomy Injury

Six WT and 6 *Wwtr1*^{+/−} mice at 6 months of age underwent phototherapeutic keratectomy (PTK). Mice were sedated, then a drop of proparacaine was applied to anesthetize the cornea and an excimer laser injury (Nidek EC-5000 Excimer Laser, average fluence of 170 mK/cm^2 with an ablation zone diameter of 2 mm and depth of 20 μm) was performed. Complete ophthalmic examinations, OCT, and ICVM were performed at baseline and on 1, 3, 5, 7, 10, and 14 days post-injury. On day 14 post-injury, all mice were euthanized and corneal endothelial wholemounts

were prepared and stained with Alizarin red as previously described.

WWTR1 Expression Levels in Human Endothelial Tissue

Expression levels of *WWTR1* and other key transcripts implicated in FECD pathogenesis were assessed in healthy human endothelial tissue from eye bank donors without the *TCF4* repeat expansion (control), presymptomatic endothelial tissue from donors with the repeat expansion (presymptomatic), endothelial tissue of patients with late-stage FECD with the repeat expansion (FECD), and endothelial tissue of patients with late-stage FECD without the repeat expansion (FECD_NR) using our previously published RNA sequencing dataset.[25]

WWTR1 Variants in FECD Patient Cohort

The study was approved by the UT Southwestern Medical Center (UTSW) Institutional Review Board (IRB) and conducted in adherence to the tenets of the Declaration of Helsinki. All study subjects were recruited at the cornea referral practice at UTSW after informed consent. Index FECD cases (probands and unrelated subjects with FECD) from the UTSW cohort were included in this study. All subjects had undergone an eye examination, including slit lamp biomicroscopy by a cornea fellowship-trained ophthalmologist (author V.V.M.) and were found to have slit lamp examination findings of grade 2 or higher on the modified Krachmer FECD grading scale.[26]

Genomic DNA was extracted from leukocytes of peripheral blood samples of subjects with Nucleon Blood Extraction Kit (Amersham, Biosciences, Buckinghamshire, UK).

The CTG18.1 trinucleotide repeat polymorphism in the *TCF4* gene was genotyped in UTSW FECD cohort of 320 probands using short tandem repeat (STR) and triplet repeat primed polymerase chain reaction (TP-PCR) assays as previously described.[27–29] For the *TCF4* trinucleotide repeat polymorphism, we dichotomized alleles such that those with 40 or more CTG triplet repeats were considered a mutant expanded allele, and those with less triplet repeats were considered a normal allele, as we have done in previous studies.[28,29]

In the subset of 96 FECD probands and 96 control subjects without the *TCF4* triplet repeat expansion, we screened for coding sequence mutations in the *WWTR1* gene by Sanger sequencing (Supplementary Table S1 with *WWTR1* primers designed using publicly available ExonPrimer software, https://ihg.helmholtz-muenchen.de/ihg/ExonPrimer.html). Variants' allele frequencies were inquired in the genome aggregation database (version 3.1.1, https://gnomad.broadinstitute.org/) and impact was predicted using PolyPhen2, (HumDiv; http://genetics.bwh.harvard.edu/pph2/) and CADD (https://cadd.gs.washington.edu/score).

Human Surgical Tissue Immunohistochemistry

Human surgical tissue explants were obtained from patients undergoing corneal transplant surgery at the University of Iowa participating in the ongoing IRB-approved Proteomic Analysis of Corneal Health study (IRB ID# 201603746). This study adheres to the tenants of the Declaration of Helsinki. None of the tissue donors procured and utilized for this investigation were from a vulnerable population, and all donors or next of kin provided appropriate consent for tissue donation and research. Human corneal endothelial tissue was placed in OptisolGS storage media (Bausch & Lomb, Irvine, CA) at 4°C right after excision from the patient's eye and fixed with 4% paraformaldehyde buffered solution, pH 7.4 for 10 minutes at room temperature within 2 to 4 hours after surgery. Control tissues were human donor corneas, processed and fixed within 14 days of procurement and were transplant suitable. Tissue was rinsed with 0.02 M PBS, pH 7.4 three times to ensure complete removal of fixative from solution. Permeabilization was achieved by 30 minutes incubation of tissue in 0.1% Triton X-100, dissolved in PBS, and followed by blocking for 1 hour at room temperature in PBS containing 2% BSA, 5% normal goat serum, and 0.1% Triton X-100. Rabbit polyclonal anti-TAZ antibody (nb110-58359, Novus Biologicals, Centennial, CO, USA) was diluted 1:200 with 0.2% BSA, 1% normal goat serum, and 0.1% Triton X-100 in PBS and applied for overnight incubation at 4°C. On the next day, tissue was washed four times with 0.1% Triton X-100 in PBS, and secondary anti-rabbit antibody conjugated to AlexaFluor488 (1:1,000, A27034, Invitrogen, Thermo Fisher Scientific, Waltham, MA, USA) and 300 nM DAPI in 0.1% Triton X-100 solution was applied for 2 hours at room temperature. Tissue was rinsed with PBS and distilled water and mounted under Aquamount mounting medium (Thermo Fisher Scientific). Images were collected by sequential confocal laser scanning microscopy using Leica SP8 STED instrument (Leica Microsystems, Mannheim, Germany).

Capillary Electrophoresis and Automated Western Blotting

Protein lysates were diluted and normalized, then mixed with a fluorescent master mix and heated at 95°C for 5 minutes. Lysates were dispensed into designated wells of a manufacturer provided microplate. Also loaded into the microplate were total protein reagent, blocking buffer, wash buffer, primary antibody (anti-TAZ/WWTR [Novus NB110-58359] diluted 1:30), secondary HRP (anti-rabbit detection module [Protein Simple DM-001]), and chemiluminescent substrate. The plate was loaded into the Jess instrument (Protein Simple) and the proteins were drawn into individual capillaries on a 13 capillary cassette (12-230 kD; SM-SW002). Data were analyzed using the Compass software provided by Protein Simple. The normalization reagent allowed the detection of total proteins in the capillary.

Statistical Analysis

Data presented as mean ± standard deviation with group wise comparisons conducted by ANOVA, Mann-Whitney *U* test, Kruskal-Wallis Test depending on distribution of the data with post hoc multiple comparisons tests (if $P < 0.05$) when appropriate (Prism 9; GraphPad Software, La Jolla, CA, USA).

Ethics Statement

All experimental procedures were in complete agreement with the ARVO Statement for the Use of Animals in Ophthalmic and Vision Research.

Results

Wwtr1 Deficient Mice Demonstrate Clinical Features of Late-Onset Fuchs' Corneal Endothelial Dystrophy

Based on a previous study[15] and recent data from our laboratory (Supplementary Fig. S1; Supplementary Materials and Methods) demonstrating a softer DM in FECD and guttae-affected patients, we sought to define the role of *WWTR1* and mechanotransduction in CEnC health and postnatal development using a *Wwtr1* KO mouse model. A *Wwtr1* breeding colony was established, resulting in 1466 viable offspring with 48.8% WT, 45.3% Het, and 5.8% KO. Similar studies have reported early mortality of KO animals due to impaired renal function.[10]

Baseline characterization of the *Wwtr1* mice revealed an overall age-related increase in mean body weight irrespective of genotype at 2 and 6 months of age, yet a significantly reduced mean body weight identified between WT (35.3 ± 9.6 g) and *Wwtr1*$^{-/-}$ (26.0 ± 5.1 g) mice by 12 months ($P = 0.01$, Supplementary Fig. S2A). There were no differences in palpebral fissure length, PRTT, IOP measurements between the different genotypes at any time point ($P > 0.05$; see Supplementary Figs. S2B, S2C, S2D). Additionally, there were no gross phenotypic corneal abnormalities identified in any of mice, irrespective of their *Wwtr1* genotype status and at any time point using slit lamp biomicroscopy with both diffuse and narrow beam illumination (see Supplementary Fig. S2E).

However, by 2 months of age, *Wwtr1*$^{-/-}$ animals had significantly reduced ECD compared with WT and *Wwtr1*$^{+/-}$ mice (2 months, WT = 2949 ± 121, *Wwtr1*$^{+/-}$ = 2920 ± 162, and *Wwtr1*$^{-/-}$ = 2456 ± 263 cells/mm^2; (Figs. 1A, 1B). Although an age-related reduction in ECD occurred in all

groups, there was a more pronounced decrease in ECD observed in the *Wwtr1*$^{+/-}$ and *Wwtr1*$^{-/-}$ mice at both the 6 (6 months, WT = 2634 ± 128, *Wwtr1*$^{+/-}$ = 2420 ± 90, and *Wwtr1*$^{-/-}$ = 2280 ± 81 cells/mm^2) and 12 month time points (12 months, WT = 2256 ± 137, *Wwtr1*$^{+/-}$ = 2152 ± 72, and *Wwtr1*$^{-/-}$ = 2059 ± 245 cells/mm^2) versus WT control mice. The CEnCs of the *Wwtr1*$^{-/-}$ had patchy and irregular reflectivity with polymegathism and a loss of cellular hexagonality compared with WT controls that worsened over time, whereas the CEnCs from *Wwtr1*$^{+/-}$ demonstrated a more intermediate phenotype between the two groups (see Fig. 1A). Despite this reduction in ECD in *Wwtr1* deficient mice, no animals developed spontaneous corneal edema by 12 months of age. There were significant differences in CCT measurements between the different groups at 2 and 12 months of age (Supplemental Figs. S3A, S3B). At 2 months, there was a significant lower CCT of *Wwtr1*$^{-/-}$ mice when compared with WT and *Wwtr1*$^{+/-}$ mice (WT = 90.3 ± 12.1, *Wwtr1*$^{+/-}$ = 90.9 ± 10.9, and *Wwtr1*$^{-/-}$ = 77.5 ± 11.3 μm), no significant differences at 6 months (WT = 98.1 ± 7.4, *Wwtr1*$^{+/-}$ = 96.8 ± 6.9, and *Wwtr1*$^{-/-}$ = 86.6 ± 6.2 μm), and at 12 months there was a significant reduction in CCT between *Wwtr1*$^{-/-}$ mice and WT mice alone (WT = 106.3 ± 7.6, *Wwtr1*$^{+/-}$ = 96.3 ± 9.3, and *Wwtr1*$^{-/-}$ = 83.6 ± 8.6 μm). This thinner cornea was largely due to a thinner cornea stroma with a subtly reduced corneal epithelial thickness also observed (see Supplementary Figs. S3A, S3C).

To assess the impact of *Wwtr1* deficiency on corneal biomechanics, AFM was performed to measure elastic modulus (tissue stiffness) of DM. At 2 months of age, there were significant differences in elastic moduli among all 3 groups with *Wwtr1*$^{-/-}$ mice having lowest DM elastic modulus (softest) followed by *Wwtr1*$^{+/-}$ and WT mice (stiffest; WT = 5.99 ± 2.03, *Wwtr1*$^{+/-}$ = 3.76 ± 0.26, and *Wwtr1*$^{-/-}$ = 1.81 ± 0.16 kPa; Fig. 2A). Older mice demonstrated a similar trend
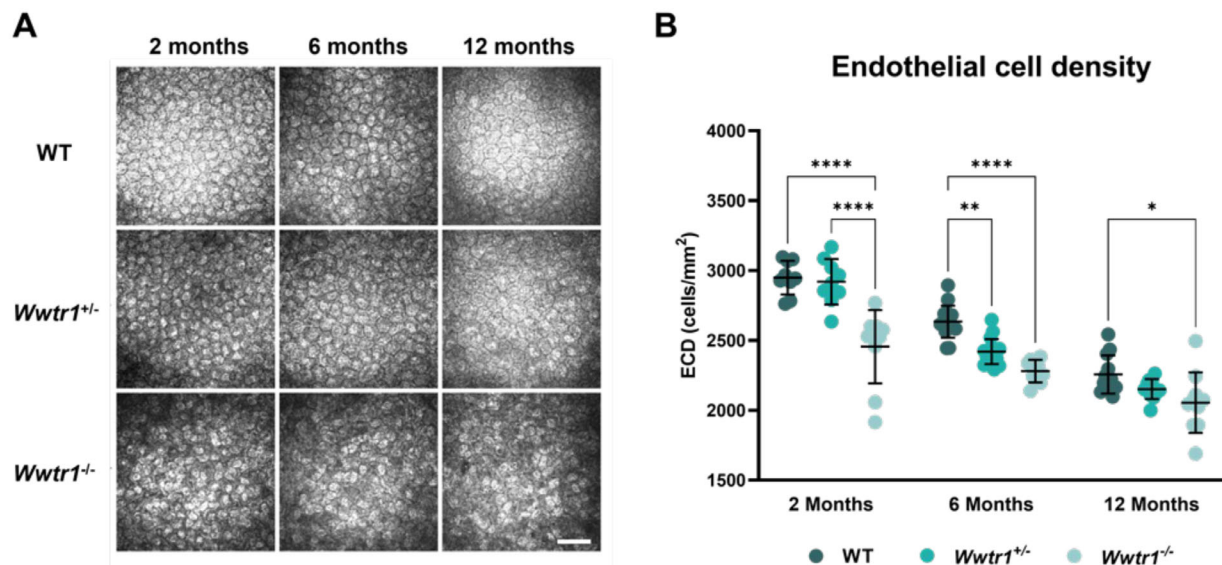

Figure 1. *Wwtr1* deficient mice exhibit reduced corneal endothelial cell density (ECD) and abnormal morphology when compared with WT controls. (**A**) In vivo confocal microscopy revealed reduced ECD in both *Wwtr1*$^{+/-}$ and *Wwtr1*$^{-/-}$ mice at 2 months compared with WT mice. Despite age-related corneal endothelial cell (CEnC) loss, *Wwtr1* deficient mice continued to have further declines in ECD at 6 and 12 months of age. Additionally, CEnCs from *Wwtr1* deficient mice demonstrated abnormal morphology, lacking the normal hexagonal shape and even distribution, and altered reflectivity when compared with WT mice. (**B**) Each dot represents the mean ECD from three representative regions in a single eye ($n \geq 9$ eyes in each group), horizonal line represents mean of the group and error bars reflect standard deviation. A 2-way ANOVA was performed to detect statistical differences, *, **, ***, **** represent $P < 0.05$, $P < 0.01$, $P < 0.001$, $P < 0.0001$, respectively. Scale bar equivalent to 50 μm.
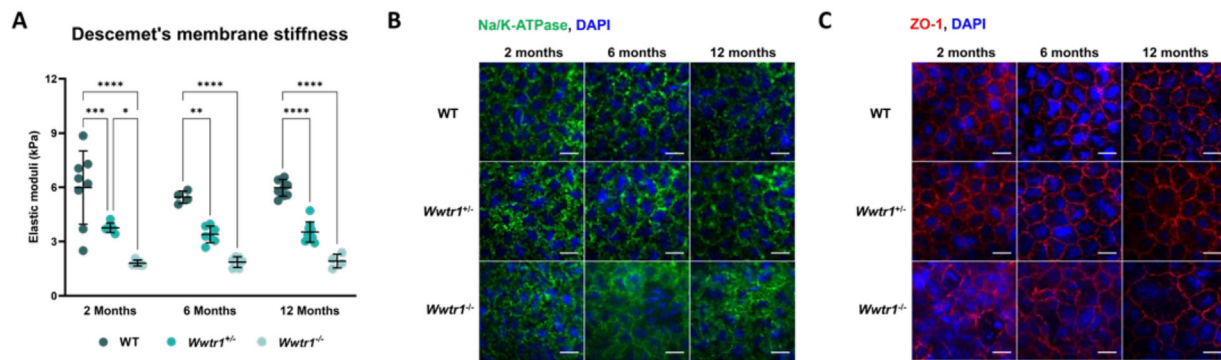
FIGURE 2. *Wwtr1* deficient mice demonstrate abnormal tissue biomechanics of Descemet's membrane and irregular protein localization in corneal endothelial cells (CEnCs) compared with WT controls. (**A**) Atomic force microscopy (AFM) performed on Descemet's membrane revealed decreased elastic modulus (softer) in *Wwtr1* deficient mice, with *Wwtr1*$^{-/-}$ mice having the lowest measurement, followed by *Wwtr1*$^{+/-}$ mice and finally WT mice (stiffest). Each dot represents a single eye ($n \geq 9$ eyes in each group with each dot representing an average elastic modulus over five locations and five force curves were generated for each location), horizonal line represents mean of the group and error bars reflect standard deviation. A 2-way ANOVA was performed to detect statistical differences, *, **, ***, **** represent $P < 0.05$, $P < 0.01$, $P < 0.001$, $P < 0.0001$, respectively. (**B, C**) Representative CEnC flatmount preparations from WT, *Wwtr1*$^{+/-}$, and *Wwtr1*$^{-/-}$ mice at 2, 6, and 12 months of age, staining for Na/K-ATPase (**B**, *green*) and ZO-1 (**C**, *red*), and nuclei (DAPI, *blue*). Both WT and *Wwtr1*$^{+/-}$ demonstrated discrete localization of Na/K-ATPase and ZO-1 to the cell periphery, whereas CEnCs from *Wwtr1*$^{-/-}$ mice had diffuse and lobulated staining for Na/K-ATPase and disrupted to absent ZO-1 staining. Scale bar equivalent to 20 μm.

with *Wwtr1* deficient mice having a softer DM compared with WT mice at 6 and 12 months of age (6 months, WT = 5.45 ± 0.34, *Wwtr1*$^{+/-}$ = 3.39 ± 0.46, and *Wwtr1*$^{-/-}$ = 1.86 ± 0.29 kPa; and 12 months, WT = 5.97 ± 0.46, *Wwtr1*$^{+/-}$ = 3.52 ± 0.56, and *Wwtr1*$^{-/-}$ = 1.92 ± 0.38 kPa).

Zonula occludens 1 (ZO-1) and Na/K-ATPase are two key proteins expressed by CEnCs and are integral to maintenance of their barrier and pump functions, respectively. Immunofluorescent staining localized Na/K-ATPase to the periphery of CEnC cytoplasm with a discrete corrugated staining pattern along the cell-cell junction in WT and *Wwtr1*$^{+/-}$ mice at all ages examined (Fig. 2B); however, *Wwtr1*$^{-/-}$ mice had a more diffuse and lobulated staining pattern along the cell border of the CEnCs. Similarly, ZO-1 staining was localized to the cell border highlighting the typical hexagonal arrangement of CEnCs in the WT and *Wwtr1*$^{+/-}$ mice (Fig. 2C). By contrast, *Wwtr1*$^{-/-}$ mice had disrupted to absent ZO-1 staining that resulted in partial loss of the hexagonal appearance of the CEnC monolayer as early as 2 months of age. Furthermore, nuclei were not evenly distributed across the corneal endothelium in *Wwtr1*$^{-/-}$ compared to WT and *Wwtr1*$^{+/-}$ mice, confirming the previous IVCM finding of polymegathism in *Wwtr1*$^{-/-}$ mice.

Wwtr1 Deficient Mice Have Impaired Corneal Wound Healing in Cryoinjury and Phototherapeutic Keratectomy Models

To test the impact of *Wwtr1* deficiency on corneal endothelial wound healing, a corneal cryoinjury model was utilized. After cryoinjury, *Wwtr1* deficient mice, both *Wwtr1*$^{+/-}$ and *Wwtr1*$^{-/-}$, demonstrated impaired wound healing characterized by large, denuded areas devoid of CEnCs on the inner aspect of DM as assessed by Alizarin red staining (Figs. 3A, 3B; WT = 0.81 ± 1.08, *Wwtr1*$^{+/-}$ = 4.45 ± 2.53, and *Wwtr1*$^{-/-}$ = 3.28 ± 3.57 mm^2); however, the only statistically significant difference was between the WT and *Wwtr1*$^{+/-}$ ($P < 0.01$). Although there were no statistically significant differences in EdU staining among the groups, there were

qualitative differences in staining distribution (Figs. 3C, 3D). Positive EdU staining was evenly distributed across the posterior cornea in WT animals; however, *Wwtr1* deficient mice had mostly peripheral EdU staining with an absence of staining in the central cornea, more pronounced in *Wwtr1*$^{-/-}$ mice compared with *Wwtr1*$^{+/-}$ mice. Additionally, impaired corneal endothelial cell wound healing was observed using a PTK model. Corneal wounds generated with the PTK laser were consistent in size, location, and depth in all treated eyes. After PTK laser treatment, *Wwtr1*$^{+/-}$ mice had delay in the return of normal CCT likely due to persistent corneal edema around post-injury day (PID) 10 that resolved by PID 14 (Figs. 4A, 4B, 4C). Indeed, corneal endothelial cell appearance (Fig. 4D) was markedly abnormal with increased CEnC reflectivity, poorly visualized nuclei and indistinct cell-cell boundaries when compared with WT mice. There was a significant reduction in ECD in *Wwtr1*$^{+/-}$ mice compared to WT controls at PID 14 when assessed using Alizarin red staining (Figs. 4E, 4F). To confirm the impairment in wound healing, Alizarin red staining was performed immediately after wounding on separate cohort of mice. In all WT mice, alizarin red staining demonstrated continuous intercellular borders in lasered and non-lasered endothelial sections (Supplementary Figs. S4A, S4B). However, *Wwtr1*$^{+/-}$ mice demonstrated discontinuity of intercellular borders, particularly within the center of the lasered endothelium. Collectively, these data suggest that *Wwtr1* deficient mice have impaired corneal endothelial wound healing with both cryogenic and laser injury.

WWTR1 is Highly Expressed in Human CEnCs, yet no Differences Were Detected in Gene Expression or Genetic Mutations Correlated With FECD-Affected Patients

Based on the findings that *Wwtr1* deficient mice recapitulate many features of late-onset FECD (decreased ECD, softer DM stiffness, abnormal subcellular localization of Na/K ATPase, and cell-cell junctional complexes), we measured the
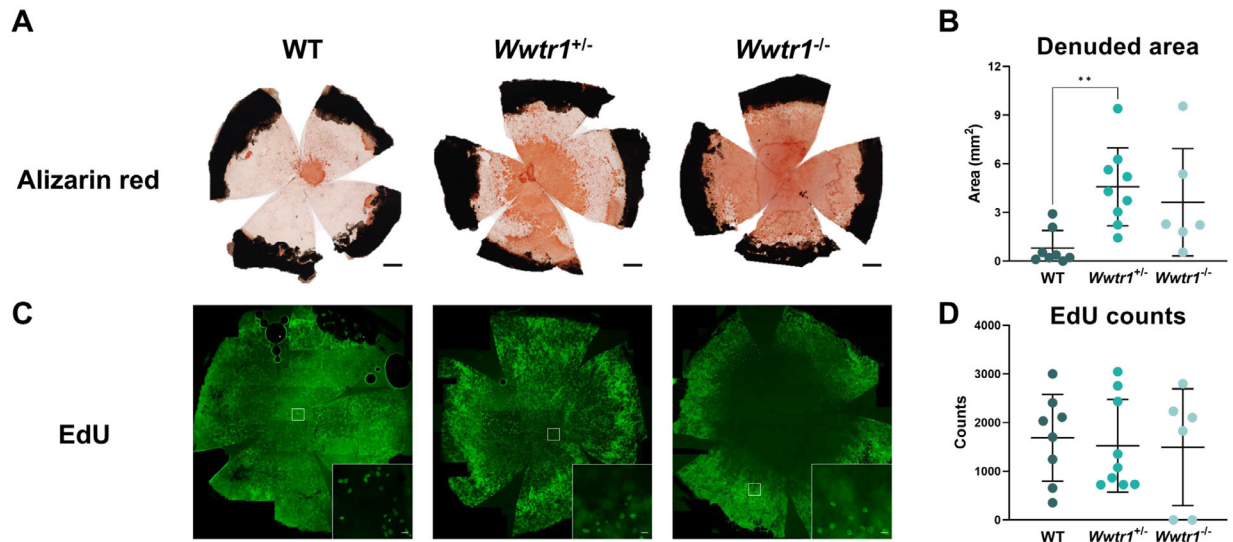
FIGURE 3. *Wwtr1* deficient mice demonstrated impaired corneal endothelial cell (CEnC) regeneration after corneal cryoinjury. A cryoinjury wound was created with a 2 mm diameter steel probe immersed in liquid nitrogen for 3 minutes (–196°C) and subsequently applied to the cornea for 10 seconds in WT ($n = 8$), *Wwtr1*$^{+/-}$ ($n = 8$), and *Wwrt1*$^{-/-}$ ($n = 5$) mice. On day 2, animals were euthanized, and the right eyes were stained with Alizarin red to calculate total denuded area (**A**) and the left eyes were stained with EdU to assess cell proliferation (**B**). (**A**) On day 2, there was a significantly larger denuded area in *Wwtr1*$^{+/-}$ mice compared with WT mice. Additionally, *Wwtr1*$^{-/-}$ mice had a trend towards larger denuded areas compared with WT mice. (**B**) There were no differences in EdU staining, indicating that the proliferative capacity of the CEnCs were equal across groups. Both Alizarin red and EdU staining were analyzed using Kruskal-Wallis tests, ** $P < 0.01$. Alizarin red scale bars equivalent to 500 µm and EdU staining scale bars equivalent to 20 µm (*inset*).
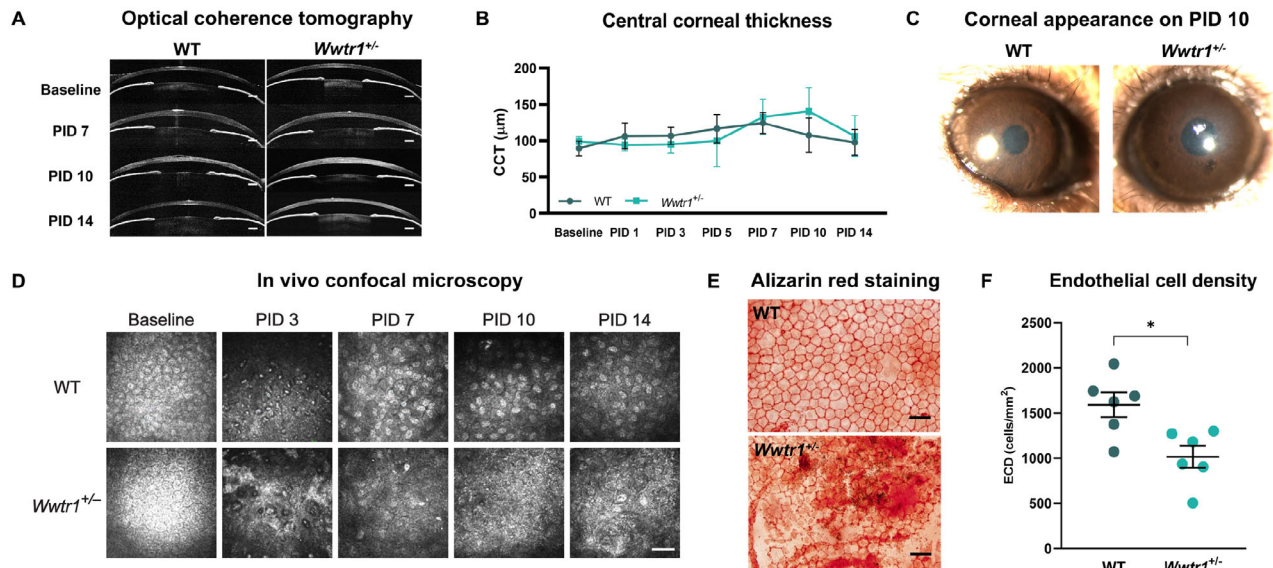

FIGURE 4. *Wwtr1* deficient mice demonstrated impaired corneal endothelial wound healing after phototherapeutic keratectomy (PTK). An endothelial wound was created with an excimer laser (20 µm depth) in 6-month-old WT ($n = 6$) and *Wwtr1*$^{+/-}$ ($n = 6$) mice. Optical coherence tomography (OCT) (**A, B**), slit lamp biomicroscopy (**C**), and in vivo confocal microscopy (IVCM) (**D**) were performed on post-injury days 1, 3, 5, 7, 10, and 14. Central corneal thickness (CCT) measured with OCT did not show statistical difference between the two genotypes (**B**), however, CCT reached its maximal thickness on post-injury days (PIDs) 7 to 10 and corneal edema was more marked on PID 10 in *Wwtr1*$^{+/-}$ mice (**C**). IVCM revealed the regenerating course of injured endothelial cells throughout the study period (**D**). Following euthanasia on PID 14, endothelial wholemounts were stained with alizarin red (**E**), and endothelial cell density (ECD) was measured. ECD was significantly reduced in *Wwtr1*$^{+/-}$ mice versus WT, suggesting impaired endothelial healing in *Wwtr1* deficient mice. CCT was analyzed using a 2-way ANOVA, ECD was analyzed using a Mann-Whitney *U* test, * $P < 0.05$. OCT scale bars equivalent to 250 µm, IVCM and Alizarin red microscopy scale bars equivalent to 50 µm.
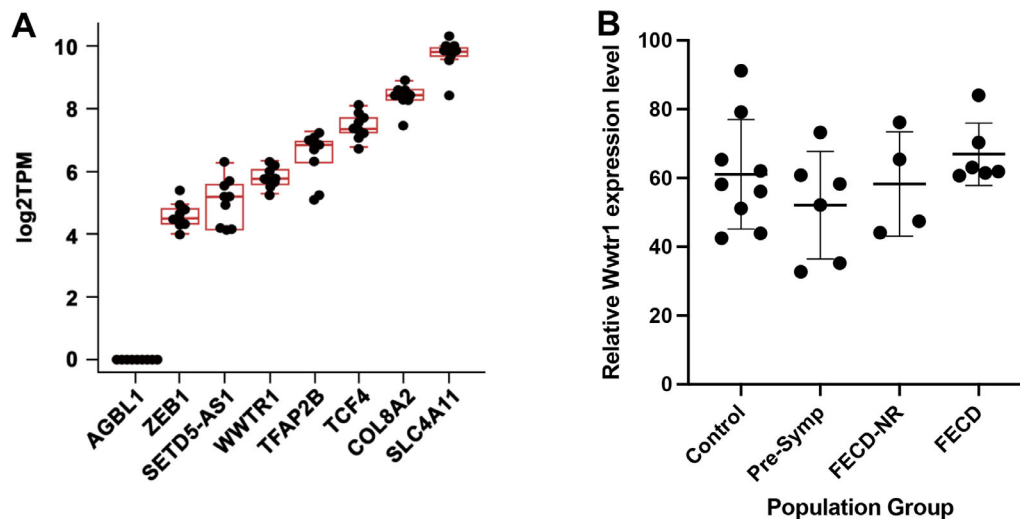
FIGURE 5. *WWTR1/TAZ expression levels are similar to that of other genes implicated in FECD.* (A) RNA was extracted from healthy human endothelial tissue from eye bank donors without the *TCF4* repeat and expression values were extracted for *WWTR1* and other genes known to play a role in FECD pathogenesis.[25] Box and whisker plot with each dot representing a single patient specimen. (**B**) RNA was extracted from healthy human endothelial tissue from eye bank donors without the *TCF4* repeat (control), presymptomatic with the repeat expansion (presymptomatic), patients with late-stage FECD without the repeat (FECD_NR), and patients with late stage FECD with the repeat (FECD). RNA sequencing was performed and *WWTR1* expression was compared across groups.[25] Each dot represents a single patient specimen, horizonal line represents mean of the group, and error bars reflect standard deviation. Data were analyzed using a Kruskal-Wallis test ($P > 0.05$).
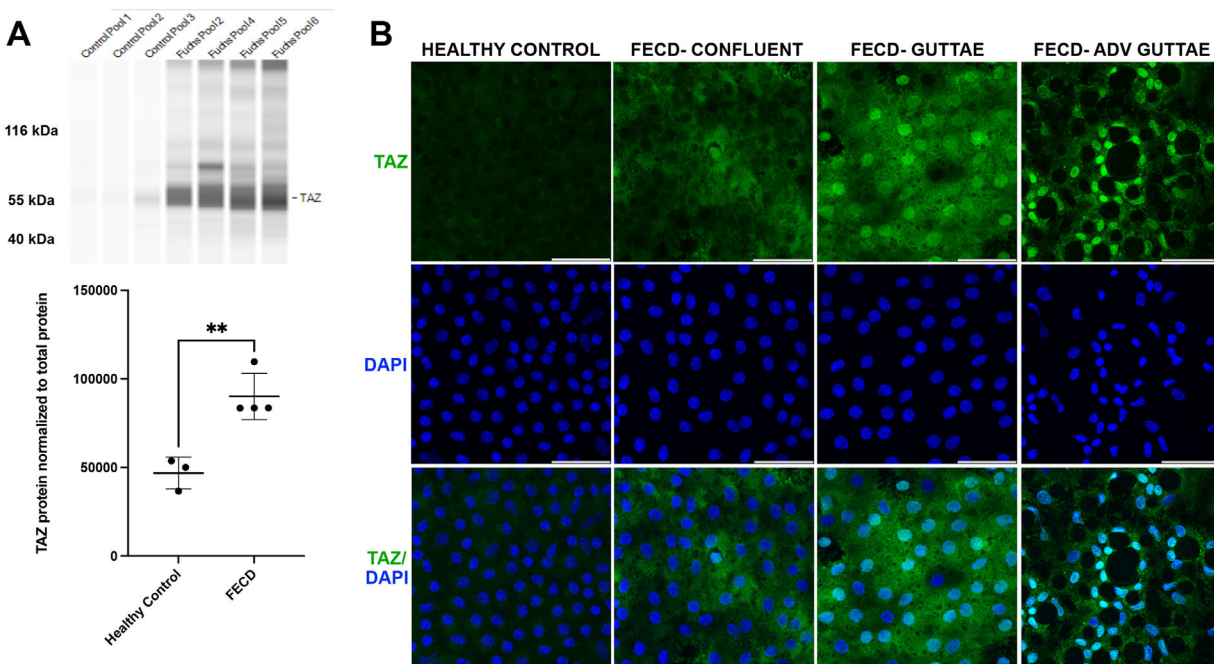

FIGURE 6. **TAZ protein expression is elevated in FECD surgical explants compared to non-FECD healthy controls.** (A) Microfluidic detection of TAZ protein in FECD surgical explants ($N = 16$, in pools of 4) had 92% higher expression of TAZ protein than non-FECD, healthy donor samples ($N = 12$, in pools of 4), where each samples' TAZ expression was normalized to total protein in that capillary (** $P = 0.0046$). (**B**) Localization of TAZ protein (*green*) in FECD surgical samples is higher in the nucleus in cells adjacent to guttae compared to cells not adjacent to guttae. As cells lose confluency, or are growing on top of developing guttae, the nuclear translocation of TAZ increases. The expression of TAZ protein is higher in immunohistochemical images of FECD samples compared to non-FECD donor samples. Images are representative samples of seven FECD and four donor controls used in the study. Nuclear counter stain = DAPI (*blue*). Scale bars are 50 µm.

expression of *WWTR1* at the gene level as well as its eight known protein-coding transcripts (Fig. 5A, Supplementary Table S2). Expression of *WWTR1* in the CEnCs of healthy human donor corneas was high and comparable to that of other genes implicated in FECD disease pathogenesis including *TCF4*, *COL8A2*, and *SLC4A11* (see Fig. 5A). We observed no statistically significant changes in *WWTR1* mRNA expression in control endothelial tissue from human donors compared to endothelial tissue samples procured from presymptomatic donors with the trinucleotide repeat expansion in the *TCF4* gene without FECD findings or patients with symptomatic late-stage FECD, with the latter group stratified based on the presence (FECD) or absence (FECD-NR) of the repeat expansion commonly identified patients with FECD (Fig. 5B).

To further explore a potential genetic role of WWTR1 in FECD-affected individuals for which a causative gene had not been identified, a genetic screen was performed on a subset of FECD-affected patients without the trinucleotide repeat expansion in *TCF4* ($n = 96$) from a larger cohort of FECD probands ($n = 320$). Among the subset, 6.1% of index cases had the Rs1055153 SNP that results in a missense mutation (p.Pro74Gln) predicted to be damaging based on PolyPhen results. However, the allele frequency of Rs1055153 was 8.9% of the control subjects (Supplementary Table S3).

WWTR1/TAZ Protein Expression is Higher in FECD-Affected Patients (Human) and Localized to the Nucleus in CEnCs Surrounding Guttae

As a master regulator of mechanotransduction, the TAZ protein can either be targeted for degradation in the cytoplasm or translocate into the nucleus to serve as a transcriptional co-activator for many genes, depending on the biomechanics of the local microenvironment. Therefore, we sought to measure TAZ protein levels and localization in CEnCs from healthy individuals and FECD-affected patients. TAZ protein expression was approximately twofold higher in FECD-affected patients compared with health individuals ($P < 0.005$; Fig. 6A). Additionally, with disease progression, TAZ moved from being primarily cytoplasmic in FECD-affected patients with a confluent CEnC monolayer to more nuclear in those with guttae (Fig. 6B). Last, FECD-affected patients with advanced guttae had nearly complete nuclear localization of TAZ. Interestingly, the nuclear localization of TAZ was most prominent in CEnCs surrounding guttae.

DISCUSSION

With the discovery of a soft DM in guttae-affected patients, we investigated the role of a key mechanotransducer, *Wwtr1*, in ocular structure and function, and CEnC wound healing. During clinical examination and imaging, we determined that *Wwtr1* deficient mice had reduced CEnC density with abnormal morphology and reduced stiffness of DM, which worsened with age. Additionally, the functional markers of CEnCs, ZO-1, and Na/K ATPase, had reduced polarization to the cell periphery suggesting abnormalities in barrier and pump function, respectively. In two injury models, cryogenic and PTK, *Wwtr1* deficient mice had impaired wound healing with persistent post-injury corneal edema and impaired CEnC regeneration. However, two key clinical features seen in late-onset FECD-affected patients not identified in *Wwtr1*

deficient mice were the presence of corneal edema and guttae. Importantly, *Wwtr1* deficient mice may have spontaneously developed corneal edema if examined at an older age (>12 months). Despite these limitations, the *Wwtr1* deficient mice recapitulate many of the clinical features of FECD, particularly aspects associated with a decrease in CEnC density and abnormalities in DM biomechanics. Therefore, we propose that the *Wwtr1* deficient mouse represents a novel model that mimics clinical features of late-onset FECD, helping to dissect the role of mechanotransduction in the pathogenesis in FECD. Studies performed with *Wwtr1* deficient mice may lead to the development of new therapeutic interventions that improve CEnC function and result in the deposition of a more normal DM with improved biomechanical properties.

The biomechanical properties of DM are dictated by both the ECM composition and the packing of the collagen fibers. Using a proteomic approach, Poulsen ET et al. characterized the protein composition of the DM/endothelial layer complex from FECD-affected patients.[30] They found 26 differentially regulated proteins in the DM/endothelial layer complex, including the downregulation of laminins and type IV collagen with an upregulation of agrin (a proteoglycan in the basal lamina) and type VI collagen, ECM proteins that comprise DM.[30] This study also identified alterations in the composition of key DM structural proteins, including decorin, type I collagen, TGF-β inducing protein, keratocan, and biglycan.[30,31] FECD-affected patients with the *TCF4* trinucleotide repeat have sequestering of RNA splicing factors, leading to mis-splicing of RNAs encoding cytoskeletal, cell adhesion, and ECM organizational proteins.[25,32–34] It has been hypothesized that the altered DM protein composition leads to more widely spaced collagen fibrils, ultimately resulting in a softer DM.[15,35] Therefore, this study sought to determine the role of mechanotransduction in CEnCs using the *Wwtr1* KO murine model.

The role of *Yap1* and *Wwtr1* in murine ocular morphology appears to be markedly different based on the observed phenotypes in the knockout mice.[9] We previously demonstrated that $Yap1^{+/-}$ mice have severe ocular abnormalities, including microphthalmia, small palpebral fissures, extensive corneal fibrosis, distorted stromal collagen fiber organization, thinning of DM, and an absent corneal endothelium.[9] By contrast, mice deficient in *Wwtr1* have relatively normal ocular structure and function with the exception of a thinner cornea in the $Wwtr1^{-/-}$ mice and reduced corneal endothelial cell density in *Wwtr1* deficient mice. Although both genes are known to be critical in organ development,[36] the major differences seen in each model highlight the disparate contributions of *Yap1* and *Wwtr1* to ocular morphology.

Despite the known genetic associations with FECD, there are few genetically modified rodent models of FECD published to study disease pathogenesis and evaluate novel therapeutic strategies.[22] Additionally, given the bidirectional nature of CEnCs and DM, there are fewer studies that investigate the relationship between abnormalities in ECM composition and FECD.[37,38] In both early- and late-onset FECD and patients with guttae, there is increased deposition of ECM components into DM, including collagens, with pathological widening of the collagen orientation resulting in softer biomechanical properties compared with the DM from healthy individuals.[15,37] Two transgenic murine strains were generated to recapitulate the common mutations L450W and Q455K in collagen type VIII alpha 2 (*COL8A2*), a major structural protein in DM,

demonstrating endothelial cell phenotypes identified in patients with early-onset FECD.[39–41] Animals with these knock-in mutations have dilated endoplasmic reticulum (ER), accumulation of misfolded proteins in the ER lumen and activation of the unfolded protein response (UPR). Importantly, these knock-in mice had reduced DM elastic modulus (softer) compared with WT mice, particularly the Q455K transgenic animals, by 5 months of age that remained reduced at 10 months in both groups.[35] This reduction in elastic modulus preceded the loss of corneal endothelial density, suggesting that abnormalities in mechanotransduction by CEnCs may play a significant role in the pathogenesis of FECD.[35] Therefore, given the similarities between the *Wwtr1* deficient mice and patients with late-onset FECD (softer DM, reduced endothelial cell density, abnormal paracellular junctions, and poor wound healing with injury), combined with abnormal mechanotransduction, the *Wwtr1* deficient mouse could serve as a novel murine model of late-onset FECD. Studies focused on the modulation of mechanotransduction could lead to the development of targeted therapeutics to reduce corneal endothelial cell dysfunction, deposit a more normal ECM, and ultimately, prevent loss of the CEnCs in FECD.

Our results suggest that *WWTR1*/TAZ is expressed in human CEnCs at levels comparable to other genes implicated in the pathogenesis of FECD including *TCF4*, *COL8A2*, and *SLC4A11*. *WWTR1* mRNA expression was equivalent when comparing healthy individuals with FECD-affected patients. However, the total TAZ protein content of CEnCs from FECD-affected patients was higher than healthy controls, suggesting that the TAZ protein had not been targeted for degradation. In FECD-affected patients with advanced guttae, there was an intense nuclear localization of TAZ in CEnCs, particularly those surrounding guttae. In other cell types, nuclear localization of TAZ has been associated with stiffer substrates, therefore, the nuclear localization in FECD-affected individuals may be the result of aberrant mechanotransduction. The molecular mechanisms underlying aberrant subcellular localization (either via changes in upstream kinases, or through associations with alternate pathways) is currently out of the scope of this paper and warrants future studies. The *Wwtr1* deficient mouse phenotype suggests that impaired mechanotransduction can result in abnormal CEnC biology, leading to CEnC cell loss, altered ECM deposition in DM, and decreased CEnC function. Therefore, we hypothesize that although no coding sequence variants in *WWTR1* associated with FECD in our cohort were identified, abnormalities in mechanotransduction may play a role in the pathogenesis of FECD.

The current study demonstrates the substantial impact of *Wwtr1* signaling on CEnC biology and the biomechanics of DM, however, there are many questions that remain unanswered. For example, what are the alterations in the CEnC transcriptomic and proteomic profile that lead to (1) altered ZO-1 and Na/K-ATPase expression and localization to the CEnC periphery, (2) reduced DM elastic modulus (softer), (3) what is the composition of DM, and (4) which factors lead to impaired wound healing. The answers to all of these questions will provide valuable insights into CEnC mechanobiology and function, with the goal to identify additional treatment options for patients with FECD.

In aggregate, this study demonstrates the impact of *Wwtr1* deficiency on ocular morphology, particularly highlighting the importance of *Wwtr1* in the maintenance of a normal CEnC structure, density, and function. Mice deficient in *Wwtr1* had decreased CEnC density, reduced elastic modulus of DM, with impaired CEnC wound healing using both cryoinjury and photo-oxidative stress. Based on the phenotypic and diagnostic similarities between *Wwtr1* deficient mice and patients with FECD, we conclude that the *Wwtr1* deficient mouse can serve as a model for late-onset FECD to (1) investigate the pathogenesis of disease and (2) develop novel therapeutic strategies.

Disclosure: **B.C. Leonard**, None; **S. Park**, None; **S. Kim**, None; **L.J. Young**, None; **I. Jalilian**, None; **K. Cosert**, None; **X. Zhang**, None; **J.M. Skeie**, None; **H. Shevalye**, None; **N. Echeverria**, None; **V. Rozo**, None; **X. Gong**, None; **C. Xing**, None; **C.J. Murphy**, None; **M.A. Greiner**, None; **V.V. Mootha**, None; **V.K. Raghunathan**, None; **S.M. Thomasy**, None

References

1. Battilana G, Zanconato F, Piccolo S. Mechanisms of YAP/TAZ transcriptional control. *Cell Stress*. 2021;5:167–172.
2. Dupont S, Morsut L, Aragona M, et al. Role of YAP/TAZ in mechanotransduction. *Nature*. 2011;474:179–183.
3. Plouffe SW, Lin KC, Moore JL, et al. The Hippo pathway effector proteins YAP and TAZ have both distinct and overlapping functions in the cell. *J Biol Chem*. 2018;293:11230–11240.
4. Raghunathan VK, Morgan JT, Dreier B, et al. Role of substratum stiffness in modulating genes associated with extracellular matrix and mechanotransducers YAP and TAZ. *Invest Ophthalmol Vis Sci*. 2013;54:378–386.
5. Muppala S, Raghunathan VK, Jalilian I, Thomasy S, Murphy CJ. YAP and TAZ are distinct effectors of corneal myofibroblast transformation. *Exp Eye Res*. 2019;180:102–109.
6. Cordenonsi M, Zanconato F, Azzolin L, et al. The Hippo transducer TAZ confers cancer stem cell-related traits on breast cancer cells. *Cell*. 2011;147:759–772.
7. Wang X, Zheng Z, Caviglia JM, et al. Hepatocyte TAZ/WWTR1 promotes inflammation and fibrosis in nonalcoholic steatohepatitis. *Cell Metab*. 2016;24:848–862.
8. Kim W, Khan SK, Gvozdenovic-Jeremic J, et al. Hippo signaling interactions with Wnt/beta-catenin and Notch signaling repress liver tumorigenesis. *J Clin Invest*. 2017;127:137–152.
9. Kim S, Thomasy SM, Raghunathan VK, et al. Ocular phenotypic consequences of a single copy deletion of the Yap1 gene (Yap1 (+/−)) in mice. *Mol Vis*. 2019;25:129–142.
10. Makita R, Uchijima Y, Nishiyama K, et al. Multiple renal cysts, urinary concentration defects, and pulmonary emphysematous changes in mice lacking TAZ. *Am J Physiol Renal Physiol*. 2008;294:F542–F553.
11. Hossain Z, Ali SM, Ko HL, et al. Glomerulocystic kidney disease in mice with a targeted inactivation of Wwtr1. *Proc Natl Acad Sci USA*. 2007;104:1631–1636.
12. Tian Y, Kolb R, Hong JH, et al. TAZ promotes PC2 degradation through a SCFbeta-Trcp E3 ligase complex. *Mol Cell Biol*. 2007;27:6383–6395.
13. Nowell CS, Odermatt PD, Azzolin L, et al. Chronic inflammation imposes aberrant cell fate in regenerating epithelia through mechanotransduction. *Nat Cell Biol*. 2016;18:168–180.

14. Wynn TA. Cellular and molecular mechanisms of fibrosis. *J Pathol*. 2008;214:199–210.

15. Xia D, Zhang S, Nielsen E, et al. The ultrastructures and mechanical properties of the Descement's membrane in Fuchs endothelial corneal dystrophy. *Sci Rep*. 2016;6:23096.

16. Tuft SJ, Coster DJ. The corneal endothelium. *Eye (Lond)*. 1990;4(Pt 3):389–424.

17. Eghrari AO, Riazuddin SA, Gottsch JD. Fuchs corneal dystrophy. *Prog Mol Biol Transl Sci*. 2015;134:79–97.

18. Ali M, Raghunathan V, Li JY, Murphy CJ, Thomasy SM. Biomechanical relationships between the corneal endothelium and Descemet's membrane. *Exp Eye Res*. 2016;152:57–70.

19. Gottsch JD, Zhang C, Sundin OH, Bell WR, Stark WJ, Green WR. Fuchs corneal dystrophy: Aberrant collagen distribution in an L450W mutant of the COL8A2 gene. *Invest Ophthalmol Vis Sci*. 2005;46:4504–4511.

20. Kocaba V, Katikireddy KR, Gipson I, Price MO, Price FW, Jurkunas UV. Association of the gutta-induced microenvironment with corneal endothelial cell behavior and demise in Fuchs endothelial corneal dystrophy. *JAMA Ophthalmol*. 2018;136:886–892.

21. Rizwan M, Peh GS, Adnan K, et al. In vitro topographical model of Fuchs dystrophy for evaluation of corneal endothelial cell monolayer formation. *Adv Healthc Mater*. 2016;5:2896–2910.

22. Park S, Leonard BC, Raghunathan VK, et al. Animal models of corneal endothelial dysfunction to facilitate development of novel therapies. *Ann Transl Med*. 2021;9:1271.

23. Morgan JT, Raghunathan VK, Thomasy SM, Murphy CJ, Russell P. Robust and artifact-free mounting of tissue samples for atomic force microscopy. *Biotechniques*. 2014;56:40–42.

24. Chang YR, Raghunathan VK, Garland SP, Morgan JT, Russell P, Murphy CJ. Automated AFM force curve analysis for determining elastic modulus of biomaterials and biological samples. *J Mech Behav Biomed Mater*. 2014;37:209–218.

25. Chu Y, Hu J, Liang H, et al. Analyzing pre-symptomatic tissue to gain insights into the molecular and mechanistic origins of late-onset degenerative trinucleotide repeat disease. *Nucleic Acids Res*. 2020;48:6740–6758.

26. Krachmer JH, Purcell JJ, Young CW, Bucher KD. Corneal endothelial dystrophy. A study of 64 families. *Arch Ophthalmol*. 1978;96:2036–2039.

27. Wieben ED, Aleff RA, Tosakulwong N, et al. A common trinucleotide repeat expansion within the transcription factor 4 (TCF4, E2-2) gene predicts Fuchs corneal dystrophy. *PLoS One*. 2012;7:e49083.

28. Mootha VV, Gong X, Ku HC, Xing C. Association and familial segregation of CTG18.1 trinucleotide repeat expansion of TCF4 gene in Fuchs' endothelial corneal dystrophy. *Invest Ophthalmol Vis Sci*. 2014;55:33–42.

29. Xing C, Gong X, Hussain I, et al. Transethnic replication of association of CTG18.1 repeat expansion of TCF4 gene with Fuchs' corneal dystrophy in Chinese implies common causal variant. *Invest Ophthalmol Vis Sci*. 2014;55:7073–7078.

30. Poulsen ET, Dyrlund TF, Runager K, et al. Proteomics of Fuchs' endothelial corneal dystrophy support that the extracellular matrix of Descemet's membrane is disordered. *J Proteome Res*. 2014;13:4659–4667.

31. Jurkunas UV, Bitar M, Rawe I. Colocalization of increased transforming growth factor-beta-induced protein (TGFBIp) and Clusterin in Fuchs endothelial corneal dystrophy. *Invest Ophthalmol Vis Sci*. 2009;50:1129–1136.

32. Wieben ED, Aleff RA, Tang X, et al. Trinucleotide repeat expansion in the transcription factor 4 (TCF4) gene leads to widespread mRNA splicing changes in Fuchs' endothelial corneal dystrophy. *Invest Ophthalmol Vis Sci*. 2017;58:343–352.

33. Fautsch MP, Wieben ED, Baratz KH, et al. TCF4-mediated Fuchs endothelial corneal dystrophy: Insights into a common trinucleotide repeat-associated disease. *Prog Retin Eye Res*. 2021;81:100883.

34. Mootha VV, Hussain I, Cunnusamy K, et al. TCF4 triplet repeat expansion and nuclear RNA foci in Fuchs' corneal dystrophy. *Invest Ophthalmol Vis Sci*. 2015;56:2003–2011.

35. Leonard BC, Jalilian I, Raghunathan VK, et al. Biomechanical changes to Descemet's membrane precede endothelial cell loss in an early-onset murine model of Fuchs endothelial corneal dystrophy. *Exp Eye Res*. 2019;180:18–22.

36. Yu FX, Zhao B, Guan KL. Hippo pathway in organ size control, tissue homeostasis, and cancer. *Cell*. 2015;163:811–828.

37. Weller JM, Zenkel M, Schlotzer-Schrehardt U, Bachmann BO, Tourtas T, Kruse FE. Extracellular matrix alterations in late-onset Fuchs' corneal dystrophy. *Invest Ophthalmol Vis Sci*. 2014;55:3700–3708.

38. Liu C, Gao ZQ, Li J, Zhou Q. Identification of novel therapeutic targets for Fuchs' endothelial corneal dystrophy based on gene bioinformatics analysis. *PLoS One*. 2022;17:e0264018.

39. Meng H, Matthaei M, Ramanan N, et al. L450W and Q455K Col8a2 knock-in mouse models of Fuchs endothelial corneal dystrophy show distinct phenotypes and evidence for altered autophagy. *Invest Ophthalmol Vis Sci*. 2013;54:1887–1897.

40. Vedana G, Villarreal G, Jun AS, Jr. Fuchs endothelial corneal dystrophy: Current perspectives. *Clin Ophthalmol*. 2016;10:321–330.

41. Jun AS, Meng H, Ramanan N, et al. An alpha 2 collagen VIII transgenic knock-in mouse model of Fuchs endothelial corneal dystrophy shows early endothelial cell unfolded protein response and apoptosis. *Hum Mol Genet*. 2012;21:384–393.